Deletion of cytosolic gating ring decreases gate and voltage sensor coupling in BK channels

Guohui Zhang,[1] Yanyan Geng,[3] Yakang Jin,[2] Jingyi Shi,[1] Kelli McFarland,[1] Karl L. Magleby,[3] Lawrence Salkoff,[4,5] and Jianmin Cui[1,2]

[1]Department of Biomedical Engineering, Center for the Investigation of Membrane Excitability Disorders, Cardiac Bioelectricity and Arrhythmia Center, Washington University, St. Louis, MO 63130
[2]Department of Pharmacology, Soochow University College of Pharmaceutical Sciences, Suzhou 215123, China
[3]Department of Physiology and Biophysics, University of Miami Miller School of Medicine, Miami, FL 33136
[4]Department of Anatomy and Neurobiology (Department of Neuroscience) and [5]Department of Genetics, Washington University School of Medicine in St. Louis, St. Louis, MO 63110

Large conductance Ca^{2+}-activated K^+ channels (BK channels) gate open in response to both membrane voltage and intracellular Ca^{2+}. The channel is formed by a central pore-gate domain (PGD), which spans the membrane, plus transmembrane voltage sensors and a cytoplasmic gating ring that acts as a Ca^{2+} sensor. How these voltage and Ca^{2+} sensors influence the common activation gate, and interact with each other, is unclear. A previous study showed that a BK channel core lacking the entire cytoplasmic gating ring (Core-MT) was devoid of Ca^{2+} activation but retained voltage sensitivity (Budelli et al. 2013. *Proc. Natl. Acad. Sci. USA*. http://dx.doi.org/10.1073/pnas.1313433110). In this study, we measure voltage sensor activation and pore opening in this Core-MT channel over a wide range of voltages. We record gating currents and find that voltage sensor activation in this truncated channel is similar to WT but that the coupling between voltage sensor activation and gating of the pore is reduced. These results suggest that the gating ring, in addition to being the Ca^{2+} sensor, enhances the effective coupling between voltage sensors and the PGD. We also find that removal of the gating ring alters modulation of the channels by the BK channel's β1 and β2 subunits.

INTRODUCTION

Large conductance BK potassium channels are activated by both voltage and intracellular calcium (Marty, 1981; Pallotta et al., 1981; Latorre et al., 1982). Opening of BK channels in muscle and neurons provides rapid efflux of potassium ion and thus hyperpolarizes the membrane potential, which provides a negative feedback to regulate membrane excitability and $[Ca^{2+}]_i$. These properties allow BK channels to play important roles in various physiological processes, such as neural excitation (Adams et al., 1982; Lancaster and Nicoll, 1987; Robitaille et al., 1993), smooth muscle contraction (Brayden and Nelson, 1992; Wellman and Nelson, 2003), hormone secretion (Petersen and Maruyama, 1984; Braun et al., 2008), hearing (Hudspeth and Lewis, 1988a,b; Wu et al., 1995), circadian rhythms (Meredith et al., 2006), and gene expression (Li et al., 2014).

BK channels are formed by four identical Slo1 subunits (Atkinson et al., 1991; Adelman et al., 1992; Shen et al., 1994; Wei et al., 1994). Each Slo1 subunit contains three distinct structural and functional domains: a voltage sensor domain (VSD) including the membrane spanning segments S1–S4 to sense membrane potential changes; a pore-gate domain (PGD), including the membrane spanning segments S5–S6 involved in opening and closing to control K^+ ion permeation; and a large cytosolic domain (CTD), containing two Ca^{2+}-binding sites (Schreiber and Salkoff, 1997; Bao et al., 2002; Shi et al., 2002; Xia et al., 2002; Zhang et al., 2010), to sense intracellular Ca^{2+}. The Slo1 subunit also contains an additional transmembrane segment S0 at the N terminus of the VSD (Meera et al., 1997). A 20–amino acid peptide (the C-Linker) covalently links the PGD and the CTD. The membrane-spanning VSD and PGD are thought to form a structure with a central pore comprised of PGD contributions from all four Slo1 subunits and four VSDs located at the periphery (Long et al., 2005; Hite et al., 2015; Tao et al., 2017). The CTD from all four subunits forms a ring-like structure known as the gating ring (Wu et al., 2010; Yuan et al., 2010, 2011) that is covalently connected to the membrane-spanning channel structure with the four C-linkers. In addition, the gating ring also makes noncovalent interactions with the VSD (Hu et al., 2003; Yang et al., 2008, 2013; Hite et al., 2017; Tao et al., 2017).

Voltage can activate BK channels in the absence of intracellular Ca^{2+}, and Ca^{2+} can activate the channel in the absence of voltage sensor activation (Meera et al.,

Correspondence to Jianmin Cui: jcui@wustl.edu
Abbreviations used: CTD, cytosolic domain; PGD, pore-gate domain; VSD, voltage sensor domain.

The Rockefeller University Press $30.00
J. Gen. Physiol. 2017 Vol. 149 No. 3 373–387
https://doi.org/10.1085/jgp.201611646

1996; Cui et al., 1997; Horrigan et al., 1999; Horrigan and Aldrich, 2002; Yang et al., 2015). These results suggest that distinct mechanisms can control the voltage- and Ca^{2+}-dependent opening of the BK channel. In contrast, Ca^{2+} affects voltage-dependent gating, whereas voltage alters Ca^{2+}-dependent gating, suggesting an interrelationship between the two mechanisms of gating (Barrett et al., 1982; Cui et al., 1997). Allosteric models have been developed to integrate both Ca^{2+} and voltage-dependent activation (Cox et al., 1997; Horrigan et al., 1999; Horrigan and Aldrich, 2002), in which three structural domains, the PGD, VSD, and CTD, can undergo separate conformational changes but also are allosterically coupled to one another, i.e., the conformation of one domain affects conformational changes in the other two. Based on this mechanism, the cytosolic gating ring may affect voltage sensor movements and the voltage-dependent opening of the channel. The interactions among VSD, PGD, and CTD are further modulated by BK channel β subunits (Niu et al., 2004), which alter the voltage- and Ca^{2+}-dependent activation (Tseng-Crank et al., 1996; Behrens et al., 2000; Orio et al., 2002).

Recently, Budelli et al. (2013) reported that a mutation of the mSlo1 channel, in which the entire CTD was replaced with an 11–amino acid Kv mini-tail (Core-MT channel), can open in response to membrane depolarization. Confirming the expectation (Xia et al., 2002, 2004), there was no Ca^{2+} sensitivity for the Core-MT channel because both proposed Ca^{2+}-binding sites located in the CTD were removed. The voltage-dependent activation was also right shifted, as might be expected if the linkers apply a passive tension to the PGD, as proposed (Niu et al., 2004). The Core-MT channel provides a tool to study the function of the gating ring in voltage-dependent activation of BK channels. It also provides an excellent opportunity to reveal the allosteric action of the CTD on the VSD and the opening of the pore and to study the interaction of β subunits.

In this study, we measure voltage sensor activation and pore opening of the Core-MT channel for comparison with WT mSlo1 over a wide range of voltages. We find that removal of the gating ring greatly alters channel opening. The open probability of Core-MT is enhanced at negative voltages but reduced at positive voltages, resulting in a shallower voltage dependence of open probability as well as a pronounced 60-mV right shift to more positive potentials for half activation. In contrast, the voltage sensor activation in Core-MT channels measured with gating currents is left shifted a small amount (−21 mV) with little effect on the voltage dependence of activation. These results indicate that the coupling between voltage sensor activation and opening of the gate is reduced in Core-MT channels. We also studied the modulation of Core-MT by β1 and β2 subunits. Our results provide insights into the interactions among structural domains of BK channel α and β subunits. The results also shed light on the mechanisms underscoring these interactions.

MATERIALS AND METHODS

Mutagenesis and expression

All mutations were made by using overlap-extension PCR with Pfu polymerase (Agilent Technologies) from the mbr5 splice variant of *mslo1* (Butler et al., 1993). All PCR-amplified regions were confirmed by sequencing. cRNA was synthesized in vitro with T3 polymerase (Ambion), and an amount of 0.05–50 or 150–250 ng/oocyte RNA for recording ionic and gating currents, respectively, was injected into oocytes (stage IV–V) from female *Xenopus laevis*. When α subunits were coexpressed with β subunits, the RNA ratio was 1:4. The WT human β1 subunit construct and inactivation-removed human β2 construct (Wallner et al., 1999; Xia et al., 2003) were used in this paper. The injected oocytes were incubated for 2–7 d at 18°C.

Electrophysiology

Inside-out patches were used to record Ionic currents with an Axopatch 200-B patch-clamp amplifier (Molecular Devices) and Pulse acquisition software (HEKA). Borosilicate pipettes with 0.5–1.5 MΩ resistance were used for inside-out patches from oocyte membrane. The current signals were then low-pass-filtered at 10 KHz and digitized at 20-µs intervals. A P/4 protocol with a holding potential of −120 mV was used to remove capacitive transients and leak currents. Solutions used in recording ionic currents were as follows. (a) Pipette solution (mM): 140 potassium methanesulfonic acid, 20 HEPES, 2 KCl, and 2 $MgCl_2$, pH 7.2. (b) The nominal 0 µM $[Ca^{2+}]_i$ solution (mM): 140 potassium methanesulfonic acid, 20 HEPES, 2 KCl, 5 EGTA, and 22 mg/liter (+)-18-crown-6-tetracarboxylic acid (18C6TA), pH 7.2. There is ∼0.5 nM free $[Ca^{2+}]_i$ in the nominal 0 $[Ca^{2+}]_i$ solution. (c) Basal bath (intracellular) solution (mM): 140 potassium methanesulfonic acid, 20 HEPES, 2 KCl, 1 EGTA, and 22 mg/liter 18C6TA, pH 7.2. $CaCl_2$ was added to the basal solution to obtain the desired free $[Ca^{2+}]_i$, which was measured by a Ca^{2+}-sensitive electrode (Thermo Fisher Scientific).

Gating currents were also recorded from inside-out patches and the currents sampled at 200 kHz and filtered at 20 kHz with leak subtraction using a −P/4 protocol. The pipette solution contained (mM) 127 TEA hydroxide, 125 methanesulfonic acid, 2 HCl, 2 $MgCl_2$, and 20 HEPES, pH 7.2, and the internal solution contained (mM) 141 NMDG, 135 methanesulfonic acid, 6 HCl, 20 HEPES, and 5 EGTA, pH 7.2. All chemicals were from Sigma-Aldrich unless otherwise noted, and all the experiments were done at room temperature (22–24°C).

Single-channel currents for Fig. 3 (A–D) were recorded at room temperature (22–25°C) with an Axopatch 200B and sampled at 200 KHz with a Digidata 1322A (Molecular Devices). Filtering for analysis was at 5 kHz. The pipette solution contained (mM) 160 KCl, 10 HEPES, 10 MES, and 2 $MgCl_2$, pH 7.0. The bath (intracellular) solution contained (mM) 160 KCl, 10 HEPES, 10 MES, and 5 HEDTA, pH 7.2. The calculated free Ca^{2+} was <3 nM based on 4.3 µM total Ca^{2+} in the solution determined by atomic absorption spectrophotometry from previous experiments. A free Ca^{2+} <3 nM is 30 times less than the 0.1 µM Ca^{2+} required to initiate activation of WT BK channels by Ca^{2+}_i (Nimigean and Magleby, 2000).

Single-channel analysis for Fig. 3 (A–D)

Core-MT channel i-V plots are based on the fully open current level. Cursor lines in Axopatch Clampfit were adjusted by eye to measure the single-channel current amplitudes (Brelidze et al., 2003). The approach used to estimate P_{OMax} for Core-MT channels is detailed in the Results. We also tried estimating P_{OMax} for Core-MT with ensemble variance analysis. The P_O was apparently too low at the highest voltage we could apply to obtain a sufficiently large number of sweeps to define a reliable fit, as might have been expected from theoretical studies (Alvarez et al., 2002; Lingle, 2006).

Further analysis

Relative conductance was determined by measuring macroscopic tail current amplitudes at −80 or −120 mV. The conductance-voltage (G-V) relationship was fitted with the Boltzmann function:

$$G/G\,Max = 1/(1+\exp(-ze\,o(V-V\,1/2)/kT)) = 1/(1+\exp((V\,1/2-V)/b)), \quad (1)$$

where G/G_{Max} represents the ratio of conductance to maximal conductance, z is the number of equivalent charges, e_o is the elementary charge, V is membrane potential, $V_{1/2}$ is the voltage where G/G_{Max} reaches 0.5, k is Boltzmann's constant, T is absolute temperature, and *b* is the slope factor with units of millivolts, where *b* gives the change in millivolts required for an e-fold change in P_O at very low P_O. Each G-V relationship was averaged from 3–15 patches, and error bars in the figures represent SEMs. SEM estimates from the Boltzmann fitting are in the figure legends.

To measure NP_O (total average open probability for all the channels N in a patch) at different negative voltage for Fig. 4 (B and C), we stimulated patches containing hundreds or thousands of channels with a long pulse (10 s) at each voltage. The currents (Fig. 4 A) were obtained by using the measured currents to subtract a baseline. All opening events were integrated (area = currents × time), which was then divided by single-channel current and total time to obtain NP_O.

The estimation of the total number of channels expressed in a membrane patch has been described previously (Horrigan et al., 1999; Cui and Aldrich, 2000) and is based on the equation

$$I = N\gamma P_O(V-E_K) = Ni. \quad (2)$$

In Eq. 2, i is single-channel current and $i = \gamma P_O(V-E_K)$. For WT *mSlo1*, N was estimated by measuring the macroscopic current at 100 mV in the presence of 100 µM $[Ca^{2+}]_i$, where the single-channel conductance is 273 pS and P_O is ∼1.0 (Yang et al., 2010). For the Core-MT mutation, we used a single-channel conductance (220 pS) and macroscopic current at 250 mV to estimate N. The P_O at this voltage was calculated based on the Boltzmann fitting of Core-MT G-V relation (Fig. 2 B; G/G_{Max} = 0.61 at 250 mV; $P_O = (G/G_{Max})P_{OMax}$), and P_{OMax} is P_O at the voltage when G/G_{Max} reaches the plateau of 1. P_{OMax} of Core-MT was assumed to be the same as E321A/E324A Core-MT (for details see Results and Fig. 3 [C and D]).

Model fitting

The HCA model (Horrigan et al., 1999) has been successfully used to describe voltage-dependent activation of BK channels. However, the HCA model does not apply to the case where the maximum open probability (P_{OMax}) is <1. To use the HCA model to describe voltage-dependent gating of Core-MT that shows a P_{OMax} <1 (see Results), we propose an extended HCA model by adding "preopen" (intermediate) states, which are closed states immediately preceding open states in gating of BK channels (Ferguson et al., 1993; Rothberg and Magleby, 1998). The preopen state is connected to the open state with a voltage-independent equilibrium constant K_1 (Scheme 1).

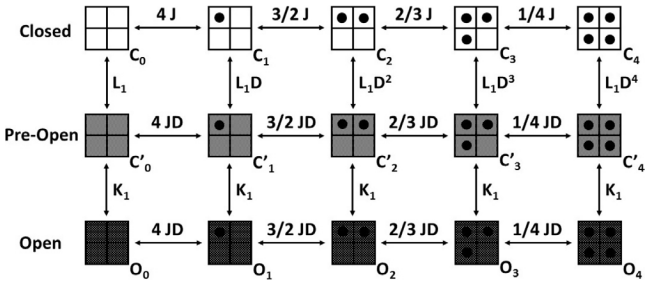

(Scheme 1)

In Scheme 1, each square represents a voltage sensor at the resting state (R), whereas each solid circle in a square represents a voltage sensor in the active state. Open squares represent the closed state (C), gray

squares represent the preopen state (C′), and dark squares represent the open state (O). The C-C′ equilibrium constant increases D-fold for each voltage sensor activated (R to A), and reciprocally, the R-A equilibrium constant increases D-fold when the channel moves from the closed state to the preopen state. Channels can be opened with an equilibrium constant K_1 after reaching the preopen state.

P_O-V curves of the WT and Core-MT channels (Figs. 4 C and 5, A–C) were fitted with the extended HCA model:

$$P_O = K_1 L_1 (1+JD)^4 / \left((1+K_1)L_1 (1+JD)^4 + (1+J)^4\right), \quad (3)$$

where

$$L_1(V) = L_1 \exp(Z_L V/kT) \quad (4)$$

$$J(V) = J_0 \exp(Z_J V/kT) = \exp\left((V - V_{hc})Z_J/kT\right) \quad (5)$$

$$D = \exp\left((V_{hc} - V_{ho})Z_J/kT\right). \quad (6)$$

L_1 is the equilibrium constant between the closed and the preopen channels ([C′]/[C]) at 0 mV, J represents the equilibrium constant for voltage sensor activation in each subunit, V_{hc} is the half-activation voltage at the closed state, V_{ho} is the half-activation voltage at the preopen state, Z_J is the charge movement during a voltage sensor activation, Z_L is the charge movement during the C to C′ transition, D is the allosteric factor coupling voltage sensor activation to channel opening, and e_o, k, T, and V were defined as in Eq. 1, where kT/e_o at 23°C = 25.5 mV. The Q_{on}-voltage plots give V_{hc} and Z_J from Boltzmann fits.

Automated fitting in Excel of the P_O-V data with Eqs. 3, 4, and 5 and fixed parameters K_1, Z_J, and V_{hc} determined directly from the experimental data then gave estimates of the fitting parameters D, Z_L, and L_1. The fitting was done by using Solver in Excel (Microsoft) with the GRC nonlinear search routine to minimize the squares of the errors between the observed and predicted P_O. Z_L and L_1 were converted to $\log_{10}$ for fitting and then converting back. Each fit was typically started several times with different starting parameters for D, Z_L, and L_1 to assure that the least squared error was obtained.

Estimates for the SEMs for D, Z_L, and L_1 for both WT and Core-MT channels were obtained by automated fitting of individual experiments with $n = 4$ for Core-MT and $n = 6$ for WT. Significance was determined with the *t* test. The data points plotted in the figures in the paper are the averages of data points from multiple experiments, and it is averaged data points that were fitted to obtain the means of the parameters presented in the paper.

RESULTS

The effects of gating ring removal on gating charge movements in BK channels

Activation of the WT mSlo1 channel depends on intracellular Ca^{2+} and voltage, and positive voltages can activate the channel in the absence of Ca^{2+} (Cui et al., 1997). The deletion of the gating ring in the Core-MT channel completely eliminated Ca^{2+} dependence of channel activation and turned the channel into a voltage-gated K^+ (Kv) channel (Budelli et al., 2013). This mutation provides an excellent opportunity to reveal the effects of the gating ring on the voltage-dependent gating of mSlo1. Voltage-dependent gating in Kv channels starts with voltage sensor activation in response to membrane depolarization. We first studied voltage sensor activation of both the WT and Core-MT channels by recording gating currents (Fig. 1). Large gating currents could be recorded from membrane patches expressing Core-MT channels (Fig. 1 A), likely reflecting the expression of a large number of the channels. The voltage for half-activation ($V_{1/2}$) of gating charge movements (Q) of Core-MT shifted 21 mV to more negative voltages relative to WT, but the slope of the Q-V relation for mutant and WT channels remained the same (Fig. 1 B). Thus, removal of the gating ring produces a small left-shift in the voltage required for voltage sensor activation, with little change in the voltage sensitivity of activation.

Deletion of the gating ring alters voltage-dependent opening of BK channels

Core-MT channels showed robust macroscopic currents at positive voltages (Fig. 2 A). Compared with WT mSlo1 channels, the voltage for half activation ($V_{1/2}$) of Core-MT channels right shifted 60 mV to more positive voltages, with a reduction in slope factor from 20.5 to 27.6 mV (Fig. 2 B). These results are consistent with those in the original study of Core-MT function (Budelli et al., 2013).

The 60-mV right shift of $V_{1/2}$ for the G-V curves of Core-MT made it technically difficult to observe the plateau of the Core-MT G-V relation because the extremely positive voltages required to reach the maximum open probability disrupted the membrane. The lack of a clear plateau made it difficult to reliably estimate $V_{1/2}$ and the slope factor by fitting the Boltzmann equation to the G-V relation (see Materials and methods). Previous work indicated that the double mutation E321A/E324A applied to WT channels left-shifted $V_{1/2}$ ~100 mV with no effect on the slope (Zhang et al., 2014). If this same mutation applied to Core-MT channels gives a similar left shift, then this would shift the activation of WT and Core-MT channels into a voltage range where the plateaus of the G-V relations of both channel types could be determined. To investigate this possibility, we mea-

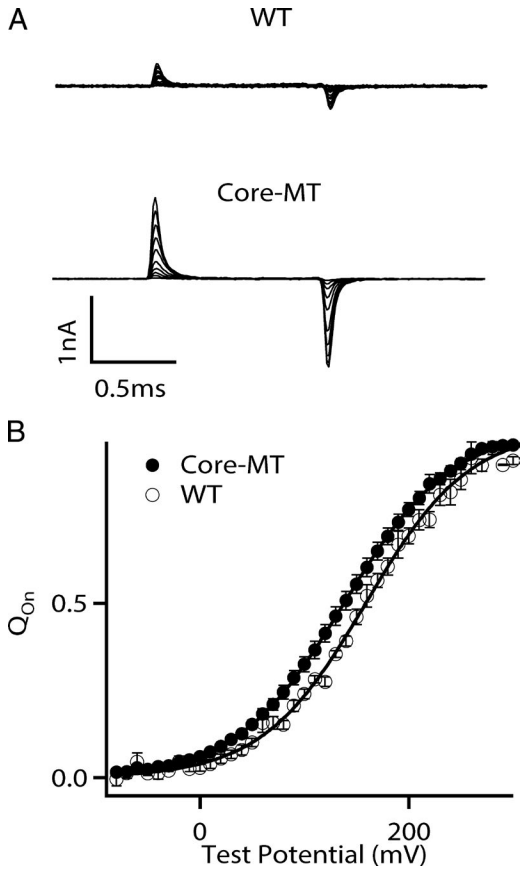

Figure 1. **Effects of gating ring removal on gating charge movements of BK channels.** (A) Gating currents of WT and Core-MT *mSlo1* channels. Voltage pulses were from −30 to 300 mV (WT) or from −80 to 300 mV (Core-MT) with 20-mV increments. (B) Normalized gating charge-voltage (Q-V) curve of on-gating currents. The smooth curves are fits to the Boltzmann function with a $V_{1/2}$ and slope factor (*b* in Eq. 1) of 159.1 ± 6.5 mV and 49.0 ± 5.9 mV for WT and 138.0 ± 3.1 mV and 51.3 ± 2.8 mV for Core-MT. $V_{1/2}$ of the on-gating current gives the half-activation voltage at the closed state, V_{hc}. The data points represent the mean ± SEM; $n \geq 4$ for all figures unless specified otherwise.

sured the G-V relations of WT and Core-MT channels with the added mutations E321A/E324A.

For both WT and Core-MT channels, the E321A/E324A mutations left-shifted $V_{1/2}$ ~100 mV with no change in slope (Fig. 2, B and D). These large left shifts allowed us to clearly observe the plateaus of the G-V curves to improve the reliability of the Boltzmann fits. For E321A/E324A mutated channels, removing the gating ring reduced the slope factor from 19.5 to 28.9 mV and right-shifted $V_{1/2}$ 73 mV (Fig. 2 D). These findings were essentially the same as for channels without the E321A/E324A mutations (Fig. 2 B). Thus, these observations indicate that with or without the E321A/E324A mutations to improve accuracy of measurement, removing the gating ring decreased the voltage sensitivity of activation and right-shifted the $V_{1/2}$ for activation. Thus, the removal of the gating ring shifts the G-V relation to more positive voltages with a reduced slope but shifts the Q-V relation in the opposite direction to more negative voltages with little change in slope.

Deleting the gating ring decreases single-channel current amplitude

Converting G-V plots to P_O-V plots requires knowing the single-channel conductance (see Materials and methods). To estimate single-channel conductance, single-channel current records were obtained from WT and Core-MT channels over a range of voltages (representative records in Fig. 3 A). For WT channels, single-channel conductance was 316 ± 5 pS at 80 mV, decreasing to 281 ± 3 pS at 160 mV; for Core-MT channels, single-channel conductance was 243 ± 3 pS at 80 mV, decreasing to 226 ± 9 pS at 160 mV (Fig. 3 B). The plot of the i-V data indicate that removing the gating ring decreased single-channel conductance a mean of 22.6 ± 1.6% over the examined voltage range of 80–160 mV. A reduced single-channel conductance for Core-MT channels has been reported previously (Budelli et al., 2013). The decline in single-channel conductance at positive voltages for WT channels mainly arises from voltage-dependent block of the pore by protons from the intracellular side (Brelidze and Magleby, 2004); a similar blocking mechanism may also apply to the Core-MT channels.

Deletion of the gating ring reduces P_{OMax} for E321A/E324A Core-MT channels

An observation that a G-V curve reaches a plateau does not indicate that the P_O of the underlying single-channels approaches 1.0 but only that the P_O has reached a maximum steady-state value, P_{OMax}. The 60-mV right shift in the G-V curve for Core-MT compared with WT (Fig. 2 B) was sufficiently large that it was not possible to collect macroscopic currents and single-channel data at sufficiently high voltages to obtain a clear plateau to estimate the P_{OMax} for Core-MT. Consequently, we took advantage of the added double mutation E321A/E324A to the Core-MT channel to left-shift the G-V curve by 90 mV (Fig. 2 D). We then measured NP_O from the single-channel current records over a range of voltages (Fig. 3, C and D), where N is the number of channels in the patch. Dividing NP_O at each voltage by the maximum number of channels simultaneously open at the highest voltage recording (≥200 mV) in the same patch then gave estimates of P_O, which was 0.21 at 200–220 mV. We then fit this P_O versus voltage relationship with a Boltzmann equation to obtain a projected P_{OMax} of 0.27 for the E321A/E324A Core-MT channel (Fig. 3 D). The observation that the macroscopic G-V curve (Fig. 2 D) and the single-channel P_O-V curve (Fig. 3 D) for E321A/E324A Core-MT channels activate and saturate over the same voltage range supports that the less

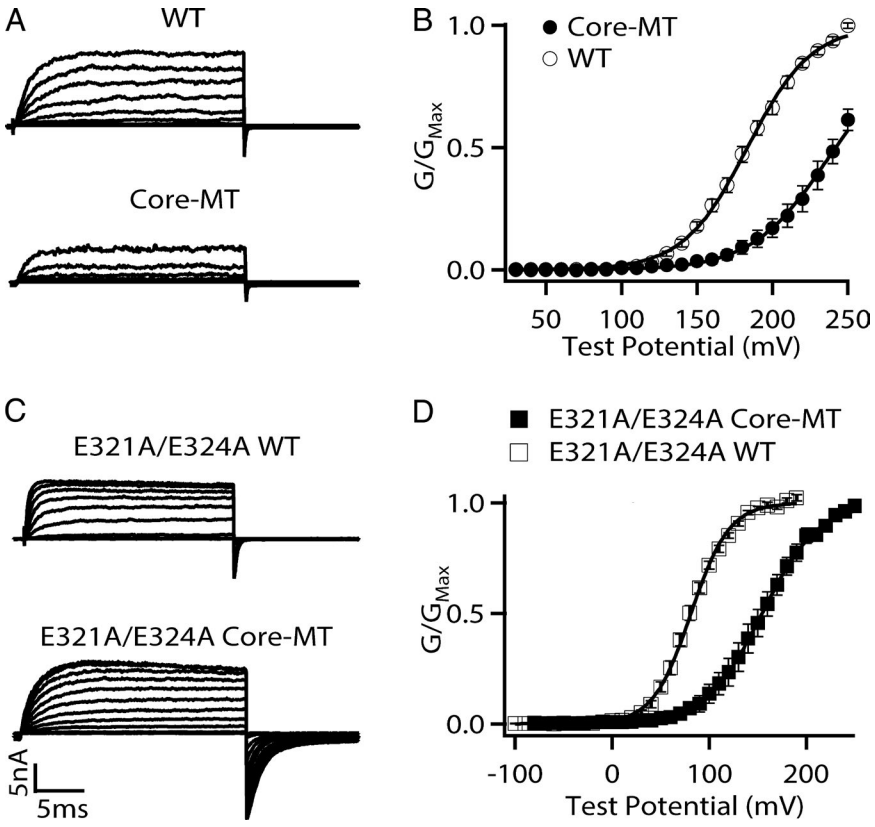

Figure 2. **Removal of gating ring alters voltage-dependent opening of BK channels.** (A) Macroscopic currents of WT and the Core-MT channels. The currents were elicited in 0 $[Ca^{2+}]_i$ by voltage pulses from −30 to 250 mV with 20-mV increments. The voltages before and after the pulses were −50 and −80 mV, respectively. (B) Conductance-voltage (G-V) curves for WT and Core-MT channels in 0 $[Ca^{2+}]_i$. Solid lines are fits to the Boltzmann relation (see Materials and methods) with $V_{1/2}$ and slope factor for WT of 184.5 ± 3.1 mV and 20.5 ± 2.8 mV and for Core-MT of 244.2 ± 3.8 mV and 27.6 ± 3.8 mV. (C) Currents of E321A/E324A WT and E321A/E324A Core-MT channels in 0 $[Ca^{2+}]_i$. (D) G-V curves for E321A/E324A WT and E321A/E324A Core-MT channels in 0 $[Ca^{2+}]_i$. Solid lines are fits to the Boltzmann relation with $V_{1/2}$ and slope factor for E321A/E324A WT of 81.3 ± 3.2 mV and 19.5 ± 2.8 mV and for E321A/E324A Core-MT of 154.4 ± 3.2 mV and 28.9 ± 2.9 mV. The data points represent the mean ± SEM; $n \geq 4$ for all figures unless specified otherwise.

well defined single-channel P_O is saturating; if the current is saturating in the macro currents, it also would be saturating in the single-channel currents. The P_{OMax} for E321A/E324A mutated WT channels approached 0.95 with Boltzmann fitting (Fig. 3 D), which is the same as P_{OMax} for WT (Horrigan et al., 1999) and in agreement of our present measurement of ∼0.94 in 0 $[Ca^{2+}]_i$), indicating that the E321A/E324A mutation added to WT did not increase, and more importantly, did not decrease P_{OMax}. If the E321A/E324A mutation added to Core-MT also does not alter P_{OMax}, then the P_{OMax} for Core-MT channels would be the same as for E321A/E324A Core-MT channels, which was 0.27. This estimate of 0.27 would place an upper limit on P_{OMax} for Core-MT channels, as estimating N by counting current levels, even for prolonged recordings, can underestimate N when P_O is small.

Deleting the gating ring increases P_O/P_{OMax} at negative potentials

G-V relations obtained from macroscopic currents (Fig. 2) can measure voltage activation for voltages where G/G_{Max} is greater than a few percent. However, previous studies have shown that the P_O of WT BK channels increases five orders of magnitude, from $\sim10^{-7}$ to ∼0.01, when voltages increase from −140 to 100 mV in 0 Ca^{2+} (Horrigan et al., 1999; Yang et al., 2010; Zhang et al., 2014). To examine to what extent the removal of the gating ring alters channel activity over these potentials, currents were recorded from membrane patches containing large numbers of WT or Core-MT channels. For such conditions, the P_O of individual channels in the membrane patch was low, but because of the large number of channels in the patch, single-channel opening events were frequently observed (Fig. 4 A). The single-channel records for WT and Core-MT channels were converted to P_O/P_{OMax} as described in the Materials and methods and plotted against membrane potential in Fig. 4 B. Deleting the gating ring increased P_O/P_{OMax} 30-fold at very negative potentials for Core-MT compared with WT.

Deletion of the gating ring reduces voltage sensor–pore coupling

In Fig. 4 C, we combine the results of the voltage dependence of channel opening measured from single-channel currents in Fig. 4 B with the macroscopic currents in Fig. 2, assuming that P_{OMax} for Core-MT channels is 0.27. Over the voltage range of ∼400 mV, P_O for WT increased $\sim10^7$-fold, whereas P_O for Core-MT increased $\sim10^5$-fold. This ∼100-fold reduction in the total increase in P_O comes from an increased P_O at negative voltages (Fig. 4 B) and a reduced P_O at positive voltages. Hence, removal of the gating ring greatly reduces the voltage dependence of channel opening. This is most easily seen by looking at the shallower slope for Core-MT compared with WT in the middle voltage range (Fig. 4 C). This marked reduction in the voltage depen-

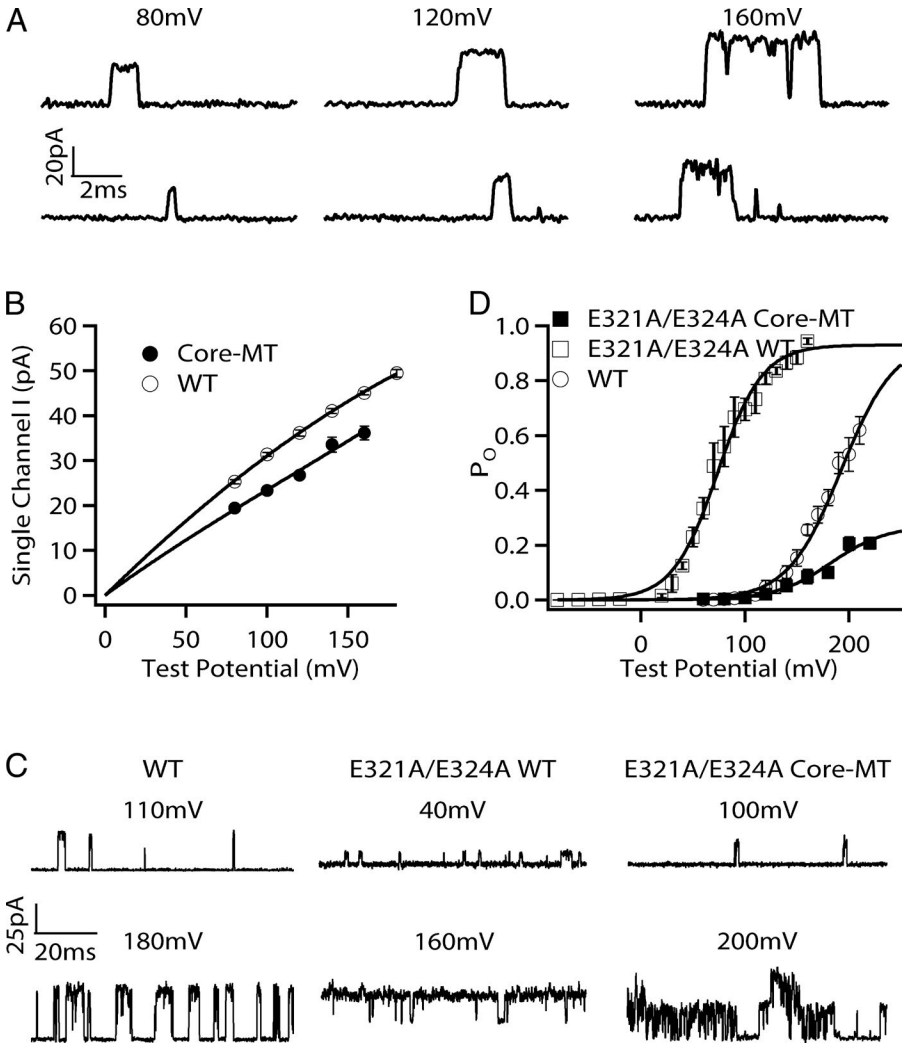

Figure 3. **Deletion of gating ring alters open probability at voltages <100 mV.** (A) Removing the CTD from *mSlo1* reduces single-channel conductance. Representative single-channel current recordings from WT (top three panels) and Core-MT (bottom three panels) at the indicated voltages obtained from inside-out patches in symmetrical 160 mM KCl. Channel openings are upwards. (B) Plots of i-V single-channel current amplitudes. The lines are cubic spline fits constrained to pass through the origin. (C) Single-channel current records at the indicated voltages from inside-out patches for WT, E321A/E324A mutated WT, and E321A/E324A mutated Core-MT as indicated. Channel openings are upwards. The activity of E321A/E324A mutated channels could wander somewhat, but much less pronounced than observed for WT *dSlo1* channels (Silberberg et al., 1996). (D) P_O increases with depolarization for the channels as indicated. The solid line is a fit to the Boltzmann function, with $V_{1/2}$ of 186.2 ± 5.4 mV, a slope factor of 21.4 ± 4.6 mV, and a P_{OMax} of 0.94 for WT; $V_{1/2}$ of 79.1 ± 4.8 mV, a slope factor of 19.3 ± 3.2 mV/e, and a P_{OMax} of 0.94 for E321A/E324A mutated WT; and $V_{1/2}$ of 182.0 ± 3.2 mV, a slope factor of 25.6 ± 2.6 mV, and a P_{OMax} of 0.27 for E321A/E324A mutated Core-MT. The number of patches for each voltage and channel type ranged from three to six. The data points represent the mean ± SEM; $n \geq 4$ for all figures unless specified otherwise.

dence of channel opening is in contrast to the small change in the voltage-dependent gating charge movements (Fig. 1 B). These results (Figs. 1, 2 B, and 4 C) indicate that the voltage sensor movements in Core-MT promote the opening of the gates less effectively than in WT. Thus, the deletion of gating ring reduces the coupling between the voltage sensor movements and gate opening in BK channels.

A quantitative description of the reduced VSD-PGD coupling in Core-MT

The experimental data in Fig. 4 clearly show that the deletion of gating ring results in an overall reduction of the VSD-pore coupling, such that the increase of channel open probability over the entire voltage range of VSD activation is reduced to ~1% of that for WT channel. It has been shown previously that voltage-dependent gating of BK channels follows an allosteric mechanism involving several molecular processes that can be well described by an allosteric HCA model (Horrigan et al., 1999). We considered using the HCA model to fit our experimental data to quantitatively describe the changes in voltage-dependent gating caused by the removal of gating ring to dissect the underlying molecular processes involved. However, the original HCA model was developed based on the WT channel in which the P_{OMax} reaches 1 so that the model does not include any mechanism that describes BK channel gating with a P_{OMax} <1.

To adopt the HCA model to fit the data from both WT and Core-MT channels, we introduce a preopen state to extend the HCA model. The experimental data are then fitted with this extended HCA model (see Materials and methods). The extended HCA model includes voltage sensor activation from the resting state to the activated state ($(R\text{-}A)_4$, for four subunits), channel opening through a preopen state C′ (C-C′-O), and the voltage sensor–pore coupling factor (D), as shown in Scheme 1. The added preopen state is a straightforward extension of the HCA model that is consistent with the experimental results of a reduced P_{OMax} for the Core-MT channel and is supported by previous experimental observations suggesting a preopen state (Ferguson et al., 1993; Rothberg and Magleby, 1998). The model as-

Table 1. **Parameters for the extended HCA model used to describe the data in Figs. 4 C and 5**

Construct	P_{OMax}	K_1	L_1	Z_L	Z_J	V_{hc}	D
				e_o	e_o	mV	
WT	0.94	15.7	3.1E-8	0.32	0.52	159	32.2
Core-MT	0.27	0.37	4.4E-5	0.38	0.50	138	4.4
Core-MT	0.99	99.0	6.1E-7	0.38	0.50	138	4.4
Core-MT	0.10	0.11	5.5E-5	0.38	0.50	138	4.4
Core-MT	0.01	0.01	6.1E-5	0.38	0.50	138	4.4

Parameters are defined in the Materials and methods. Z_L and Z_J have units of electronic charge, e_o.

sumes that activation of the VSD does not open the channel directly but increases the occupancy of the preopen state, which increases P_O via an intrinsic voltage-independent transition.

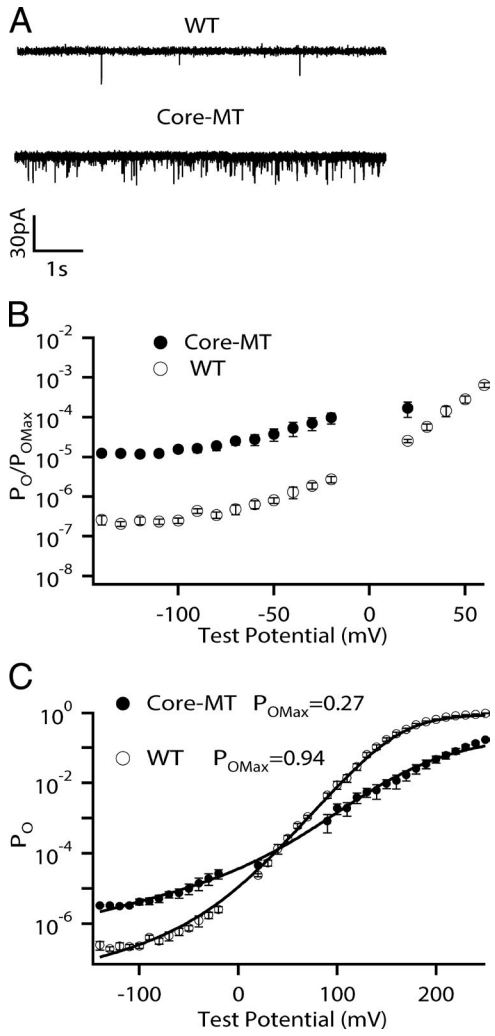

Figure 4. **P_O-V relations of WT and mutated channels.** (A) Unitary channel openings at −140 mV from membrane patches containing multiple channels. (B) P_O/P_{OMax}-V relations at 0 $[Ca^{2+}]_i$. (C) Plot of P_O versus voltage for WT and Core-MT channels. The smooth curves are fits to the extended HCA model with P_{OMax} = 0.27 for Core-MT and P_{OMax} = 0.94 for WT. The data points represent the mean ± SEM; $n \geq 4$ for all figures unless specified otherwise.

At high voltage where G/G_{Max} reaches a plateau, $(1 + J)^4 << (1 + JD)^4$, then

$$P_{OMax} = K_1/(1 + K_1).$$

From our measurements where P_{OMax} = 0.94 for WT channels and 0.27 for Core-MT channels, we obtain K_1= 15.7 for WT channels and 0.37 for Core-MT channels (Table 1). Estimates of V_{hc} and Z_J were obtained from the Q-V plots in Fig. 1 B, and then the P_O-V data were fit to the extended HCA model with an automatic fitting algorithm (see Materials and methods) to obtain estimates of the free parameters L_1, Z_L, and D (Table 1), which are generally similar for WT to those from previous HCA model fittings (Horrigan et al., 1999; Zhang et al., 2010), considering that the models could have different constraints. Comparing the values of the fitted parameters of the WT and Core-MT channels, we found that the removal of gating ring alters various aspects of voltage-dependent gating of the channels (Fig. 4 C and Table 1). Most notably, D, the equilibrium factor that drives the gating from the closed to the preopen closed states in Scheme 1 and also facilitates voltage sensor activation for preopen states, decreased significantly from 32.2 ± 3.0 for WT to 4.4 ± 1.1 ($P < 0.0001$) for Core-MT. L_1, the intrinsic equilibrium between the closed and preopen state, increased significantly from $3.10^{-8} \pm 0.4 \times 10^{-8}$ in WT to $4.4 \times 10^{-5} \pm 0.7 \times 10^{-5}$ in Core-MT ($P < 0.005$). Removing the gating ring had an insignificant effect on Z_L, the effective charge movement associated with transitions from the closed to the preopen (intermediate) state, which was 0.32 ± 0.02 e_o in WT and 0.38 ± 0.10 e_o in Core-MT ($P > 0.11$).

For Fig. 4 C, we used an indirect estimate of 0.27 for P_{OMax} for Core-MT based on studies with E321A/E324A mutations of WT and Core-MT channels (Fig. 3, C and D). To explore to what extent potential errors in estimating P_{OMax} would have on estimates of the coupling factor D and other parameters, we present three plots for assumed P_{OMax} for Core-MT channels of 0.99, 0.1, and 0.01 (Fig. 5). In all three plots, the slopes of the Core-MT channel were similar and less than for WT, indicating reduced voltage sensitivity over the wide range of explored values for P_{OMax}. The plots were then fitted with the extended HCA model. We found that the value

of P_{OMax} for Core-MT did not affect the D factor (Fig. 5 and Table 1) but altered L_1 and K_1 to shift the plots up and down. These results further support our observations (Fig. 4 C and Table 1) that the removal of gating ring reduces D, the voltage sensor–gate coupling.

To explore whether potential errors in estimating Z_L could give rise to apparent uncoupling of voltage sensors from gates, we fixed Z_L to various values and then refit the P_O versus V curve of Core-MT with L_1 and D as free parameters. Fixing Z_L from its best-fit value of 0.38 e_o to 0.1, 0.2, 0.5, or 0.8 e_o and refitting changed D from its best-fit value of 4.4 to 10.5, 7.7, 3.0, and 1.1, respectively. Consequently, over a greater range of values of Z_L for Core-MT than might be expected, estimates of D for Core-MT remained greatly reduced compared with 32.2 for WT, indicating that the observed uncoupling does not arise from possible errors in estimating Z_L. It also should be noted that the fits became worse when Z_L was fixed away from its best-fit value.

We also explored whether possible errors in determining L_1 could have induced the decrease in D for Core-MT channels. Fixing L_1 threefold higher or threefold lower than the best fitting value for Core-MT data and refitting the Core-MT data changed D to 1.86 or 9.2, respectively, compared with 32.2 for WT. Consequently, for a wide range of possible errors in estimating L_1, removing the gating ring still uncoupled the voltage sensors from the gates. Hence, the extended data analyses in these sections and the SEM of the fitted parameters and *t* tests in a previous section all quantitatively indicate that removal of the gating ring uncoupled the PGD from the VSD in terms of the extended HCA model.

Deletion of gating ring increases the intrinsic open probability, P_{OInt}, of BK channels at negative voltage

BK channels can still open at very negative voltages (less than or equal to −100 mV) where the voltage dependence of the open probability becomes shallower (Fig. 4 C; Horrigan et al., 1999; Yang et al., 2010). These observations suggest that the channel has an intrinsic open probably, P_{OInt}, at very negative potentials that is not dependent on voltage sensor activation. Based on our estimate of P_{OMax} for Core-MT channels of 0.27, the intrinsic P_{OInt} at negative voltages for Core-MT was 15-fold higher than that of WT (Fig. 4 C).

From Scheme 1, it can be seen that a decreased coupling factor D would have no effect at very negative voltages. Consequently, the extended HCA model accounts for the 15-fold increase in P_{OInt} at very negative potentials through changes in the parameters K_1, L_1, and Z_L, with the major change being a large increase in L_1, the equilibrium for the C-C′ transition at 0 mV. As the voltage is increased, the decreased coupling between voltage sensors and gate (D) in Core-MT gives a decreased voltage sensitivity, so P_O increases at a slower rate in

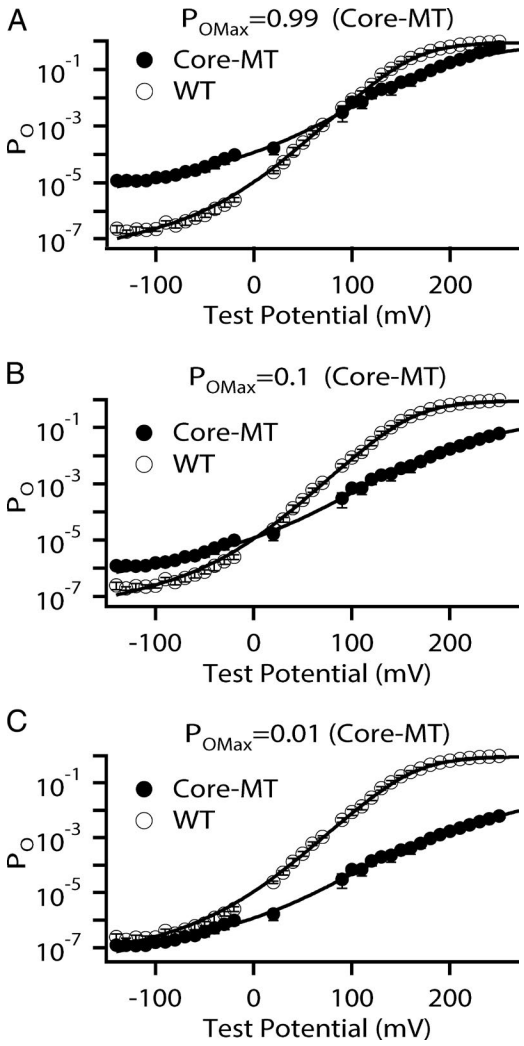

Figure 5. **Plots of P_O versus voltage for WT and Core-MT channels.** (A–C) The Core-MT data have been scaled assuming that P_{OMax} for Core-MT channels is 0.99, 0.1, and 0.01, as indicated in A–C, respectively. P_{OMax} was always 0.94 for WT channels. The smooth curves are fits to the extended HCA model with the parameters in Table 1. The voltage sensitivity of P_O versus voltage (slope) of the scaled Core-MT data was always less than for the WT data, indicating that the observation of decreased coupling for Core-MT was independent of the assumed value for P_{OMax}. The data points represent the mean ± SEM; $n \geq 4$ for all figures unless specified otherwise.

Core-MT reaching a lower P_O. The extended HCA model tells us how K_1, L_1, and Z_L change in terms of the highly simplified model but gives little information about the multiple transduction pathways and energy barriers thought to be involved in voltage sensor–PGD coupling (Horrigan and Aldrich, 2002; Niu et al., 2004; Sweet and Cox, 2008; Hite et al., 2017) and how these would be altered by removing the gating ring.

Setting the model aside, the experimental observations are that removing the gating ring increases P_O at negative voltages and decreases P_O at positive voltages and decreases the coupling between voltage sensors

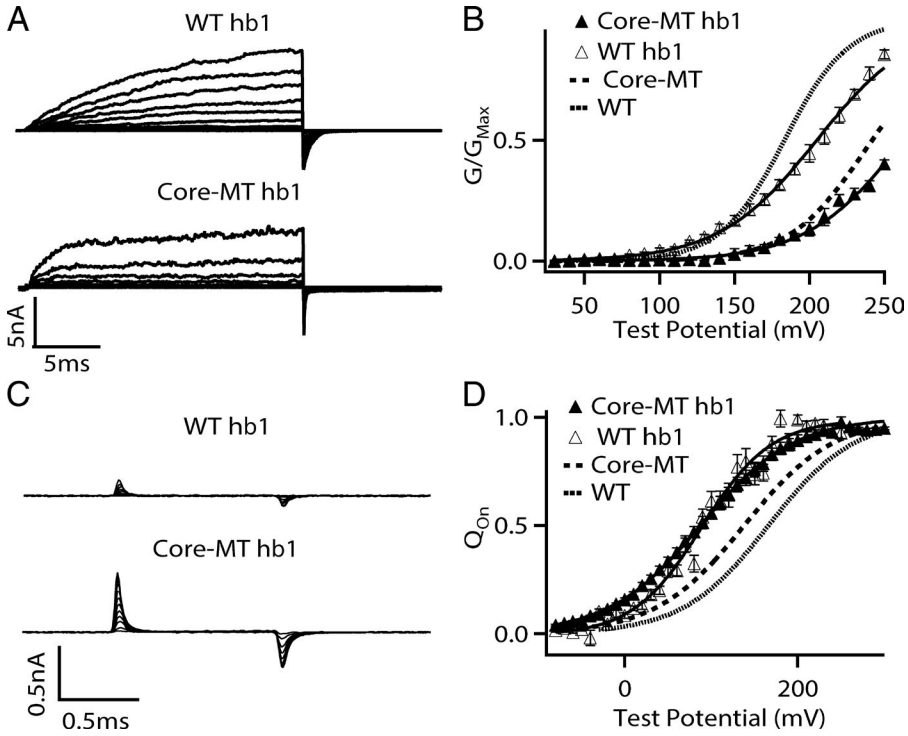

Figure 6. **β1 subunit modulates voltage-dependent activation.** (A) Macroscopic current traces were elicited in 0 $[Ca^{2+}]_i$ by voltage pulses from −30 to 250 mV with 20-mV increments. The voltages before and after the pulses were −50 and −80 mV, respectively. (B) G-V curves for WT + hβ1 and Core-MT + hβ1 channels in 0 $[Ca^{2+}]_i$. Solid lines are fits to the Boltzmann equation with $V_{1/2}$ and slope factor for WT + hβ1 of 205.0 ± 4.7 mV and 32.6 ± 4.8 mV and for Core-MT + hβ1 of 262.8 ± 6.2 mV and 32.2 ± 6.1 mV. (C) Gating current traces for WT + hβ1 and Core-MT + hβ1. Voltage pulses were from −30 to 300 mV (WT + hβ1) or from −80 to 300 mV (Core-MT + hβ1) in 20-mV increments. (D) Normalized Q-V relations of on-gating currents. The smooth curves are fits to the Boltzmann equation with $V_{1/2}$ and slope factor 88.8 ± 6.8 mV and 40.1 ± 5.2 mV for WT + hβ1 and 87.6 ± 5.0 mV and 53.3 ± 4.3 mV for Core-MT + hβ1. The data points represent the mean ± SEM; $n \geq 4$ for all figures unless specified otherwise.

and gates. As a possible mechanism, at very negative voltages the intrinsic open probability of Core-MT channels is higher than for WT channels because the fully resting (held down) voltage sensors are only partially coupled to the gates, so the gates are not held as fully closed. Hence, the decreased coupling between voltage sensors and gates after removing the gating ring would have a dual effect on BK channel gating, decreasing P_O at positive potentials and increasing P_O at negative potentials.

Deletion of gating ring alters β subunit modulation

β1 and β2 subunits of BK channels interact with mSlo1 to alter Ca^{2+} and voltage-dependent activation. Their modulation of voltage-dependent activation of mSlo1 can be measured in 0 $[Ca^{2+}]_i$, with a different phenotype for the β1 and β2 subunits (Orio et al., 2002; Lee and Cui, 2009; Lee et al., 2010). The β1 subunit shifts the G-V relationship to the right and reduces slope, whereas the β2 subunit does not alter the G-V relation (Figs. 6 B and 7 B; Orio et al., 2002). In contrast, both β subunits alter gating charge movements by shifting the Q-V relation to more negative voltages (Figs. 6 D and 7 D; Sun et al., 2013). Previous studies suggest that β1 and β2 subunits also modify voltage-dependent activation via different mechanisms. It is thought that β1 mainly interacts with the voltage sensor of *Slo1* to alter Q-V directly, whereas β2 primarily interacts with the cytosolic gating ring to alter Q-V indirectly (Lee and Cui, 2009; Lee et al., 2010; Sun et al., 2013). Here, we study the Core-MT channel to further test these previously proposed mechanisms.

Fig. 6 A shows the current traces of WT and Core-MT with the coexpression of human β1 subunit (hβ1). Compared with WT + hβ1, Core-MT + hβ1 currents activated with faster kinetics. However, β1 altered the G-V relation of Core-MT and WT in a similar manner, by reducing the steepness and shifting the G-V to more positive voltages (Fig. 6 B). β1 left-shifted the Q-V of both WT and Core-MT to more negative voltages (Bao and Cox, 2005). The −50-mV left shift for Core-MT Q-V was less than the −70 mV left shift for WT Q-V (Fig. 6, C and D; and Fig. 1 B). Interestingly, the Q-V of WT + hβ1 and that of Core-MT + hβ1 were nearly superimposable. This result could indicate that the gating ring has no effect on β1–voltage sensor interactions.

The β2 subunit had no effects on the G-V relation of WT or Core-MT (Fig. 7, A and B). β2 left-shifted the Q-V relation of Core-MT to more negative voltages by −22 mV, which was less than the left shift of −65 mV for WT (Fig. 7, C and D; and Fig. 1 B). Thus, the removal of the gating ring had a small effect on the modulation of G-V and Q-V relations by β1 but a larger effect on the modulation of Q-V relation by β2. These results are consistent with the previously proposed mechanisms that β1 mainly interacts with the voltage sensor of *mSlo1* to modify voltage-dependent gating, whereas β2 primarily interacts with the gating ring to indirectly modify voltage-dependent gating.

DISCUSSION

We have studied voltage-dependent activation of the Core-MT mutation and found that the deletion of the

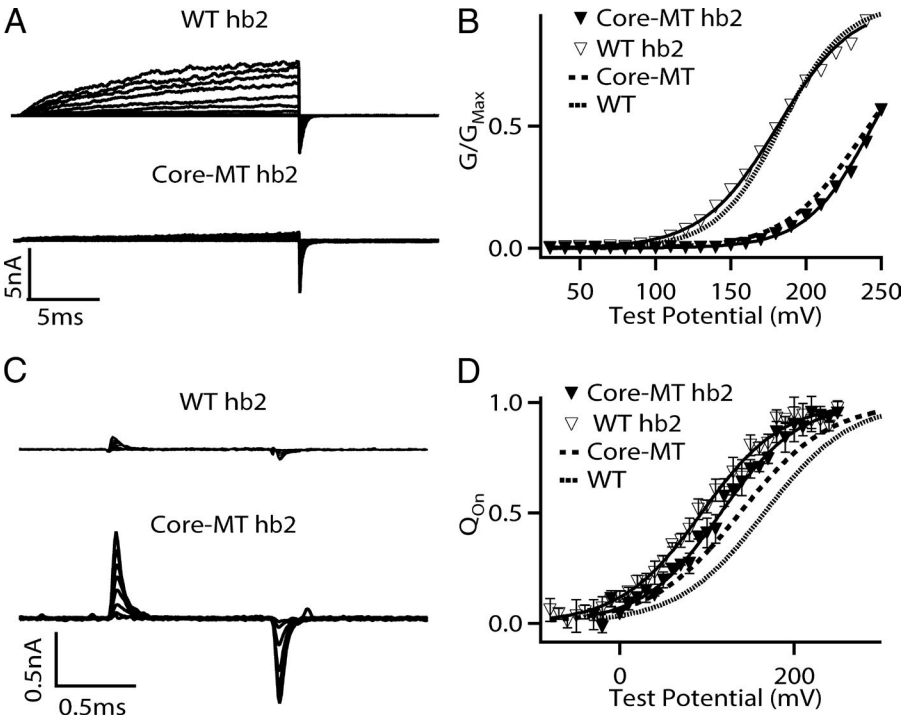

Figure 7. **β2 subunit modulates voltage-dependent activation.** (A) Macroscopic current traces were elicited in 0 $[Ca^{2+}]_i$ by voltage pulses from −30 to 250 mV with 20-mV increments. The voltages before and after the pulses were −50 and −80 mV, respectively. (B) G-V relations for WT + hβ2 and Core-MT + hβ2 in 0 $[Ca^{2+}]_i$. Solid lines are fits to the Boltzmann equation with $V_{1/2}$ and slope factor for WT + hβ2 of 181.3 ± 3.4 mV and 24.9 ± 3.1 mV and for Core-MT + hβ2 of 244.3 ± 3.0 mV and 22.0 ± 3.1 mV. (C) Gating current traces for WT + hβ2 and Core-MT + hβ2. Voltage pulses were from −30 to 300 mV for WT + hβ2 and from −80 to 300 mV for Core-MT + hβ2 in 20-mV increments. (D) Normalized Q-V relations of on-gating currents. The smooth curves are fits to the Boltzmann equation with $V_{1/2}$ and slope factor 94.2 ± 6.1 mV and 46.1 ± 5.1 mV for WT + hβ2 and 116.2 ± 6.1 mV and 44.9 ± 5.4 mV for Core-MT + hβ2. The data points represent the mean ± SEM; $n \geq 4$ for all figures unless specified otherwise.

gating ring from mSlo1 channels had a small effect on voltage sensor movement, left-shifting $V_{1/2}$ of the Q_{On}-V relation −21 mV with negligible change in slope (Fig. 1). In contrast, the deletion of the gating ring decreased the voltage dependence of channel opening. The open probability of the WT mSlo1 channel increased ∼4×10^6–fold over the 400-mV test potential range of −140 to 260 mV, whereas the open probability of the Core-MT mutation increased ∼5×10^4–fold over the same voltage range, being reduced ∼100-fold (Fig. 4 C). This result indicates that the deletion of the gating ring weakens the coupling between the VSDs and the PGD to reduce the influence of voltage sensor activation on pore opening. Fitting the data with an extended HCA model showed a significant reduction of the D factor, which measures the VSD-pore coupling, from 32.2 in WT to 4.4 in Core-MT (Fig. 4 C and Table 1).

The change in channel open probability caused by the removal of gating ring was observed over the wide examined voltage range, with an increase of intrinsic opening of BK channels at voltages where the voltage sensors would be in the resting state and a decrease in the maximum open probability that the channel can attain at high voltages where the voltage sensors would be fully activated (Fig. 4 C). These results are consistent with a proposed model in which the PGD coupled with the VSD has an intrinsic open probability for negative potentials in 0 Ca^{2+}_i and that, normally in WT channels, the VSD-pore coupling suppresses pore opening, decreasing the intrinsic opening probability when the VSDs are in the resting state at negative potentials but promotes pore opening when the VSDs are at the activated state at positive potentials. Because the gating ring in WT BK channels facilitates the VSD-pore coupling, the removal of the gating ring in Core-MT shows the dual effect of increasing P_O at more negative potentials and decreasing P_O at more positive potentials. This is evident in the crossing of the P_O/voltage curves for WT and Core-MT channels at ∼40 mV in Fig. 4 C.

The BK channel gating ring contains eight Ca^{2+}-binding sites that mediate Ca^{2+}-dependent opening of the channel (Schreiber and Salkoff, 1997; Shi et al., 2002; Xia et al., 2002, 2004; Wu et al., 2010; Yuan et al., 2010, 2011; Zhang et al., 2010; Hite et al., 2017; Tao et al., 2017). Previous studies have shown that, although depolarizing voltages and Ca^{2+} binding can independently open BK channels (Cui et al., 1997), Ca^{2+} binding affects voltage-dependent opening, and likewise, voltage depolarization alters Ca^{2+}-dependent opening (Horrigan and Aldrich, 2002; Sweet and Cox, 2008). This interdependence of voltage and Ca^{2+}-dependent channel opening could be caused by a direct interaction between the voltage sensor and Ca^{2+} binding site, or alternatively, linked by the interactions among VSD, PGD, and gating ring that are responsible for the facilitation of VSD-pore coupling by the gating ring. Therefore, a conformational change in VSD could affect the conformation of the gating ring and vice versa.

What are the interactions among VSD, PGD, and gating ring that are responsible for the facilitation of VSD-pore coupling by the gating ring? Previous studies have revealed three types of interactions among the three domains. The first interaction is a direct pull between gating ring and the pore-gate through C-linkers. This

interaction is supported by the observation that a shortening or lengthening of C-linkers from the PGD to the gating ring by deletion or addition of amino acid residues altered voltage and Ca^{2+} dependences of BK channel opening; the alteration was dependent on the length of the C-linker and could be explained as if the C-linker–gating ring complex behaved like a passive spring in 0 Ca^{2+}, pulling on the PGD to open the channels (Niu et al., 2004). Recently solved structures of the BK channel in both apo and Ca^{2+}-bound states showed that Ca^{2+} binding expands the top of the gating ring, consistent with the idea that C-linkers from the gating ring to the S6 helices in the PGD are pulled upon Ca^{2+} binding (Yuan et al., 2010, 2011; Hite et al., 2017; Tao et al., 2017).

Pull on the C-linkers is coupled in the gating ring with an elevation of the α-B helix of each subunit of the gating ring (Yuan et al., 2010, 2011; Hite et al., 2017; Tao et al., 2017). This elevated α-B helix could push directly on the VSD-PGD providing a second type of interaction among the three domains. Push on the VSD-PGD may activate the channel directly. This push by the α-B helix on the VSD-PGD could also push the gating ring away from the VSD-PGD increasing the pull of the C-linkers on the S6 helices to further activate the channel through a push-pull mechanism.

The third type of interaction involves electrostatic interaction directly between the gating ring and the VSD. In studies of Mg^{2+}-dependent activation of BK channels, it was found that the putative Mg^{2+}-binding site was located in the interface between the VSD and gating ring, with two residues from each of the domains (D99 and N172 from the VSD and E374 and E399 from the gating ring) forming Mg^{2+} coordinators (Yang et al., 2008). The bound Mg^{2+} activates the channel by electrostatic interaction with R213 in the S4 transmembrane segment of the VSD (Hu et al., 2003). These studies indicate a close proximity between the gating ring and the VSD and identified interactions between pairs of residues in the two domains, including spontaneously formed disulfide bond between C99 and C397, residues D99–E374, and charges at 172–399 (Yang et al., 2008, 2013). The crystal structures of BK channel gating ring show that E374 and E399 locate at the top surface of the gating ring, which faces the membrane, providing further support to these functional findings (Wu et al., 2010; Yuan et al., 2010, 2011).

With any of the above mechanisms, the interaction between the gating ring and the membrane-spanning domains could have a profound effect on the conformations of the membrane-spanning domain because removal of the gating ring not only reduces the VSD-PGD coupling but also alters the intrinsic energy for channel opening. Our gating current measurements showed that removal of the gating ring shifted V_{hc}, the half activation voltage for the closed states, −21 mV, from 159 mV for WT to 138 mv for Core-MT. This shift would arise from changes in the VSD movements when the channels were still closed (Scheme 1 [top row], Fig. 1, and Table 1). To determine the effect of gating ring removal on V_{ho}, the voltage for half activation for the preopen states (second row in Scheme 1), Eq. 6 (see Materials and methods) was arranged to obtain:

$$V_{ho} = V_{hc} - (kT/Z_J)\ln D.$$

The large decrease in D upon removing the gating right-shifted V_{ho} 73 mV, from −11 mV for WT to 62 mV for Core-MT. The much larger shift in V_{ho} compared with the shift in V_{hc} suggests that removal of the gating ring may primarily affect the conformation of the preopen states rather than that of the closed states. This idea is consistent with the changes of the intrinsic energy for transitions of the preopen state to the closed (L_1) or open (K_1) state. In terms of the extended HCA model, it is mainly the shift in V_{ho} for the preopen states that shifts the G/G_{Max}-V curve.

The effect of the mini tail (11 amino acids of C-linker) remaining after removing the gating ring (see Materials and methods) on the voltage-dependent gating of Core-MT channels is not known. For example, the mini tails might themselves interact, altering the gating process. The contribution of the mini tail to our observed Core-MT behavior needs to be examined when a method is devised to express Core channels without the mini tail, to fully evaluate the effects of the gating ring in BK channel gating.

In summary, removing the gating ring of the BK channel had profound effects of reducing the increase of probability of channel opening while only inducing a small leftward shift in the voltage required for activation of the gating current. These observations indicate that removing the gating ring decreases coupling between voltage sensors and the gates. Thus, the gating ring normally contributes to coupling, even in the absence of Ca^{2+}. Our results also support the mechanism that the β2 subunit, but not the β1 subunit, alters BK channel voltage sensor movements primarily by interacting with the gating ring.

ACKNOWLEDGMENTS

This work was supported by National Institutes of Health grants R01 HL70393 and R01 NS092570 to J. Cui and R01 GM114694 to L. Salkoff and K.L. Magleby and National Natural Science Foundation of China grant 31271143 to J. Cui.

The authors declare no competing financial interests.

Richard W. Aldrich served as editor.

Submitted: 18 June 2016
Revised: 28 October 2016
Accepted: 28 December 2016

REFERENCES

Adams, P.R., A. Constanti, D.A. Brown, and R.B. Clark. 1982. Intracellular Ca^{2+} activates a fast voltage-sensitive K^+ current in vertebrate sympathetic neurones. *Nature.* 296:746–749. http://dx.doi.org/10.1038/296746a0

Adelman, J.P., K.Z. Shen, M.P. Kavanaugh, R.A. Warren, Y.N. Wu, A. Lagrutta, C.T. Bond, and R.A. North. 1992. Calcium-activated potassium channels expressed from cloned complementary DNAs. *Neuron.* 9:209–216. http://dx.doi.org/10.1016/0896-6273(92)90160-F

Alvarez, O., C. Gonzalez, and R. Latorre. 2002. Counting channels: a tutorial guide on ion channel fluctuation analysis. *Adv. Physiol. Educ.* 26:327–341. http://dx.doi.org/10.1152/advan.00006.2002

Atkinson, N.S., G.A. Robertson, and B. Ganetzky. 1991. A component of calcium-activated potassium channels encoded by the *Drosophila* slo locus. *Science.* 253:551–555. http://dx.doi.org/10.1126/science.1857984

Bao, L., and D.H. Cox. 2005. Gating and ionic currents reveal how the BK_{Ca} channel's Ca^{2+} sensitivity is enhanced by its β1 subunit. *J. Gen. Physiol.* 126:393–412. http://dx.doi.org/10.1085/jgp.200509346

Bao, L., A.M. Rapin, E.C. Holmstrand, and D.H. Cox. 2002. Elimination of the BK_{Ca} channel's high-affinity Ca^{2+} sensitivity. *J. Gen. Physiol.* 120:173–189. http://dx.doi.org/10.1085/jgp.20028627

Barrett, J.N., K.L. Magleby, and B.S. Pallotta. 1982. Properties of single calcium-activated potassium channels in cultured rat muscle. *J. Physiol.* 331:211–230. http://dx.doi.org/10.1113/jphysiol.1982.sp014370

Behrens, R., A. Nolting, F. Reimann, M. Schwarz, R. Waldschütz, and O. Pongs. 2000. hKCNMB3 and hKCNMB4, cloning and characterization of two members of the large-conductance calcium-activated potassium channel β subunit family. *FEBS Lett.* 474:99–106. http://dx.doi.org/10.1016/S0014-5793(00)01584-2

Braun, M., R. Ramracheya, M. Bengtsson, Q. Zhang, J. Karanauskaite, C. Partridge, P.R. Johnson, and P. Rorsman. 2008. Voltage-gated ion channels in human pancreatic β-cells: electrophysiological characterization and role in insulin secretion. *Diabetes.* 57:1618–1628. http://dx.doi.org/10.2337/db07-0991

Brayden, J.E., and M.T. Nelson. 1992. Regulation of arterial tone by activation of calcium-dependent potassium channels. *Science.* 256:532–535. http://dx.doi.org/10.1126/science.1373909

Brelidze, T.I., and K.L. Magleby. 2004. Protons block BK channels by competitive inhibition with K^+ and contribute to the limits of unitary currents at high voltages. *J. Gen. Physiol.* 123:305–319. http://dx.doi.org/10.1085/jgp.200308951

Brelidze, T.I., X. Niu, and K.L. Magleby. 2003. A ring of eight conserved negatively charged amino acids doubles the conductance of BK channels and prevents inward rectification. *Proc. Natl. Acad. Sci. USA.* 100:9017–9022. http://dx.doi.org/10.1073/pnas.1532257100

Budelli, G., Y. Geng, A. Butler, K.L. Magleby, and L. Salkoff. 2013. Properties of Slo1 K^+ channels with and without the gating ring. *Proc. Natl. Acad. Sci. USA.* 110:16657–16662. http://dx.doi.org/10.1073/pnas.1313433110

Butler, A., S. Tsunoda, D.P. McCobb, A. Wei, and L. Salkoff. 1993. mSlo, a complex mouse gene encoding "maxi" calcium-activated potassium channels. *Science.* 261:221–224. http://dx.doi.org/10.1126/science.7687074

Cox, D.H., J. Cui, and R.W. Aldrich. 1997. Allosteric gating of a large conductance Ca-activated K^+ channel. *J. Gen. Physiol.* 110:257–281. http://dx.doi.org/10.1085/jgp.110.3.257

Cui, J., and R.W. Aldrich. 2000. Allosteric linkage between voltage and Ca^{2+}-dependent activation of BK-type mslo1 K^+ channels. *Biochemistry.* 39:15612–15619. http://dx.doi.org/10.1021/bi001509+

Cui, J., D.H. Cox, and R.W. Aldrich. 1997. Intrinsic voltage dependence and Ca^{2+} regulation of mslo large conductance Ca-activated K^+ channels. *J. Gen. Physiol.* 109:647–673. http://dx.doi.org/10.1085/jgp.109.5.647

Ferguson, W.B., O.B. McManus, and K.L. Magleby. 1993. Opening and closing transitions for BK channels often occur in two steps via sojourns through a brief lifetime subconductance state. *Biophys. J.* 65:702–714. http://dx.doi.org/10.1016/S0006-3495(93)81097-X

Hite, R.K., P. Yuan, Z. Li, Y. Hsuing, T. Walz, and R. MacKinnon. 2015. Cryo-electron microscopy structure of the Slo2.2 Na^+-activated K^+ channel. *Nature.* 527:198–203. http://dx.doi.org/10.1038/nature14958

Hite, R.K., X. Tao, and R. MacKinnon. 2017. Structural basis for gating the high-conductance Ca^{2+}-activated K^+ channel. *Nature.* 541:52–57. http://dx.doi.org/10.1038/nature20775

Horrigan, F.T., and R.W. Aldrich. 2002. Coupling between voltage sensor activation, Ca^{2+} binding and channel opening in large conductance (BK) potassium channels. *J. Gen. Physiol.* 120:267–305. (published erratum appears in *J. Gen. Physiol.* 2002. 120:599) http://dx.doi.org/10.1085/jgp.20028605

Horrigan, F.T., J. Cui, and R.W. Aldrich. 1999. Allosteric voltage gating of potassium channels I. Mslo ionic currents in the absence of Ca^{2+}. *J. Gen. Physiol.* 114:277–304. http://dx.doi.org/10.1085/jgp.114.2.277

Hu, L., J. Shi, Z. Ma, G. Krishnamoorthy, F. Sieling, G. Zhang, F.T. Horrigan, and J. Cui. 2003. Participation of the S4 voltage sensor in the Mg^{2+}-dependent activation of large conductance (BK) K^+ channels. *Proc. Natl. Acad. Sci. USA.* 100:10488–10493. http://dx.doi.org/10.1073/pnas.1834300100

Hudspeth, A.J., and R.S. Lewis. 1988a. Kinetic analysis of voltage- and ion-dependent conductances in saccular hair cells of the bull-frog, *Rana catesbeiana*. *J. Physiol.* 400:237–274. http://dx.doi.org/10.1113/jphysiol.1988.sp017119

Hudspeth, A.J., and R.S. Lewis. 1988b. A model for electrical resonance and frequency tuning in saccular hair cells of the bull-frog, *Rana catesbeiana*. *J. Physiol.* 400:275–297. http://dx.doi.org/10.1113/jphysiol.1988.sp017120

Lancaster, B., and R.A. Nicoll. 1987. Properties of two calcium-activated hyperpolarizations in rat hippocampal neurones. *J. Physiol.* 389:187–203. http://dx.doi.org/10.1113/jphysiol.1987.sp016653

Latorre, R., C. Vergara, and C. Hidalgo. 1982. Reconstitution in planar lipid bilayers of a Ca^{2+}-dependent K^+ channel from transverse tubule membranes isolated from rabbit skeletal muscle. *Proc. Natl. Acad. Sci. USA.* 79:805–809. http://dx.doi.org/10.1073/pnas.79.3.805

Lee, U.S., and J. Cui. 2009. β subunit-specific modulations of BK channel function by a mutation associated with epilepsy and dyskinesia. *J. Physiol.* 587:1481–1498. http://dx.doi.org/10.1113/jphysiol.2009.169243

Lee, U.S., J. Shi, and J. Cui. 2010. Modulation of BK channel gating by the β2 subunit involves both membrane-spanning and cytoplasmic domains of Slo1. *J. Neurosci.* 30:16170–16179. http://dx.doi.org/10.1523/JNEUROSCI.2323-10.2010

Li, B., W. Jie, L. Huang, P. Wei, S. Li, Z. Luo, A.K. Friedman, A.L. Meredith, M.H. Han, X.H. Zhu, and T.M. Gao. 2014. Nuclear BK channels regulate gene expression via the control of nuclear calcium signaling. *Nat. Neurosci.* 17:1055–1063. http://dx.doi.org/10.1038/nn.3744

Lingle, C.J. 2006. Empirical considerations regarding the use of ensemble-variance analysis of macroscopic currents. *J. Neurosci. Methods.* 158:121–132. http://dx.doi.org/10.1016/j.jneumeth.2006.05.027

Long, S.B., E.B. Campbell, and R. Mackinnon. 2005. Voltage sensor of Kv1.2: structural basis of electromechanical coupling. *Science.* 309:903–908. http://dx.doi.org/10.1126/science.1116270

Marty, A. 1981. Ca-dependent K channels with large unitary conductance in chromaffin cell membranes. *Nature.* 291:497–500. http://dx.doi.org/10.1038/291497a0

Meera, P., M. Wallner, Z. Jiang, and L. Toro. 1996. A calcium switch for the functional coupling between α (*hslo*) and β subunits ($K_{V,\ Ca}\beta$) of maxi K channels. *FEBS Lett.* 382:84–88. http://dx.doi.org/10.1016/0014-5793(96)00151-2

Meera, P., M. Wallner, M. Song, and L. Toro. 1997. Large conductance voltage- and calcium-dependent K^+ channel, a distinct member of voltage-dependent ion channels with seven N-terminal transmembrane segments (S0-S6), an extracellular N terminus, and an intracellular (S9-S10) C terminus. *Proc. Natl. Acad. Sci. USA.* 94:14066–14071. http://dx.doi.org/10.1073/pnas.94.25.14066

Meredith, A.L., S.W. Wiler, B.H. Miller, J.S. Takahashi, A.A. Fodor, N.F. Ruby, and R.W. Aldrich. 2006. BK calcium-activated potassium channels regulate circadian behavioral rhythms and pacemaker output. *Nat. Neurosci.* 9:1041–1049. http://dx.doi.org/10.1038/nn1740

Nimigean, C.M., and K.L. Magleby. 2000. Functional coupling of the β_1 subunit to the large conductance Ca^{2+}-activated K^+ channel in the absence of Ca^{2+}. Increased Ca^{2+} sensitivity from a Ca^{2+}-independent mechanism. *J. Gen. Physiol.* 115:719–736. http://dx.doi.org/10.1085/jgp.115.6.719

Niu, X., X. Qian, and K.L. Magleby. 2004. Linker-gating ring complex as passive spring and Ca^{2+}-dependent machine for a voltage- and Ca^{2+}-activated potassium channel. *Neuron.* 42:745–756. http://dx.doi.org/10.1016/j.neuron.2004.05.001

Orio, P., P. Rojas, G. Ferreira, and R. Latorre. 2002. New disguises for an old channel: MaxiK channel β-subunits. *News Physiol. Sci.* 17:156–161.

Pallotta, B.S., K.L. Magleby, and J.N. Barrett. 1981. Single channel recordings of Ca^{2+}-activated K^+ currents in rat muscle cell culture. *Nature.* 293:471–474. http://dx.doi.org/10.1038/293471a0

Petersen, O.H., and Y. Maruyama. 1984. Calcium-activated potassium channels and their role in secretion. *Nature.* 307:693–696. http://dx.doi.org/10.1038/307693a0

Robitaille, R., M.L. Garcia, G.J. Kaczorowski, and M.P. Charlton. 1993. Functional colocalization of calcium and calcium-gated potassium channels in control of transmitter release. *Neuron.* 11:645–655. http://dx.doi.org/10.1016/0896-6273(93)90076-4

Rothberg, B.S., and K.L. Magleby. 1998. Kinetic structure of large-conductance Ca^{2+}-activated K^+ channels suggests that the gating includes transitions through intermediate or secondary states. A mechanism for flickers. *J. Gen. Physiol.* 111:751–780. http://dx.doi.org/10.1085/jgp.111.6.751

Schreiber, M., and L. Salkoff. 1997. A novel calcium-sensing domain in the BK channel. *Biophys. J.* 73:1355–1363. http://dx.doi.org/10.1016/S0006-3495(97)78168-2

Shen, K.Z., A. Lagrutta, N.W. Davies, N.B. Standen, J.P. Adelman, and R.A. North. 1994. Tetraethylammonium block of Slowpoke calcium-activated potassium channels expressed in *Xenopus* oocytes: evidence for tetrameric channel formation. *Pflugers Arch.* 426:440–445. http://dx.doi.org/10.1007/BF00388308

Shi, J., G. Krishnamoorthy, Y. Yang, L. Hu, N. Chaturvedi, D. Harilal, J. Qin, and J. Cui. 2002. Mechanism of magnesium activation of calcium-activated potassium channels. *Nature.* 418:876–880. http://dx.doi.org/10.1038/nature00941

Silberberg, S.D., A. Lagrutta, J.P. Adelman, and K.L. Magleby. 1996. Wanderlust kinetics and variable Ca^{2+}-sensitivity of *Drosophila*, a large conductance Ca^{2+}-activated K^+ channel, expressed in oocytes. *Biophys. J.* 70:2640–2651. http://dx.doi.org/10.1016/S0006-3495(96)79833-8

Sun, X., J. Shi, K. Delaloye, X. Yang, H. Yang, G. Zhang, and J. Cui. 2013. The interface between membrane-spanning and cytosolic domains in Ca^{2+}-dependent K^+ channels is involved in β subunit modulation of gating. *J. Neurosci.* 33:11253–11261. http://dx.doi.org/10.1523/JNEUROSCI.0620-13.2013

Sweet, T.-B., and D.H. Cox. 2008. Measurements of the BK_{Ca} channel's high-affinity Ca^{2+} binding constants: effects of membrane voltage. *J. Gen. Physiol.* 132:491–505. http://dx.doi.org/10.1085/jgp.200810094

Tao, X., R.K. Hite, and R. MacKinnon. 2017. Cryo-EM structure of the open high-conductance Ca^{2+}-activated K^+ channel. *Nature.* 541:46–51. http://dx.doi.org/10.1038/nature20608

Tseng-Crank, J., N. Godinot, T.E. Johansen, P.K. Ahring, D. Strøbaek, R. Mertz, C.D. Foster, S.P. Olesen, and P.H. Reinhart. 1996. Cloning, expression, and distribution of a Ca^{2+}-activated K^+ channel beta-subunit from human brain. *Proc. Natl. Acad. Sci. USA.* 93:9200–9205. http://dx.doi.org/10.1073/pnas.93.17.9200

Wallner, M., P. Meera, and L. Toro. 1999. Molecular basis of fast inactivation in voltage and Ca^{2+}-activated K^+ channels: a transmembrane β-subunit homolog. *Proc. Natl. Acad. Sci. USA.* 96:4137–4142. http://dx.doi.org/10.1073/pnas.96.7.4137

Wei, A., C. Solaro, C. Lingle, and L. Salkoff. 1994. Calcium sensitivity of BK-type K_{Ca} channels determined by a separable domain. *Neuron.* 13:671–681. http://dx.doi.org/10.1016/0896-6273(94)90034-5

Wellman, G.C., and M.T. Nelson. 2003. Signaling between SR and plasmalemma in smooth muscle: sparks and the activation of Ca^{2+}-sensitive ion channels. *Cell Calcium.* 34:211–229. http://dx.doi.org/10.1016/S0143-4160(03)00124-6

Wu, Y.C., J.J. Art, M.B. Goodman, and R. Fettiplace. 1995. A kinetic description of the calcium-activated potassium channel and its application to electrical tuning of hair cells. *Prog. Biophys. Mol. Biol.* 63:131–158. http://dx.doi.org/10.1016/0079-6107(95)00002-5

Wu, Y., Y. Yang, S. Ye, and Y. Jiang. 2010. Structure of the gating ring from the human large-conductance Ca^{2+}-gated K^+ channel. *Nature.* 466:393–397. http://dx.doi.org/10.1038/nature09252

Xia, X.M., X. Zeng, and C.J. Lingle. 2002. Multiple regulatory sites in large-conductance calcium-activated potassium channels. *Nature.* 418:880–884. http://dx.doi.org/10.1038/nature00956

Xia, X.M., J.P. Ding, and C.J. Lingle. 2003. Inactivation of BK channels by the NH_2 terminus of the β2 auxiliary subunit: an essential role of a terminal peptide segment of three hydrophobic residues. *J. Gen. Physiol.* 121:125–148. http://dx.doi.org/10.1085/jgp.20028667

Xia, X.M., X. Zhang, and C.J. Lingle. 2004. Ligand-dependent activation of Slo family channels is defined by interchangeable cytosolic domains. *J. Neurosci.* 24:5585–5591. http://dx.doi.org/10.1523/JNEUROSCI.1296-04.2004

Yang, H., J. Shi, G. Zhang, J. Yang, K. Delaloye, and J. Cui. 2008. Activation of Slo1 BK channels by Mg^{2+} coordinated between the voltage sensor and RCK1 domains. *Nat. Struct. Mol. Biol.* 15:1152–1159. http://dx.doi.org/10.1038/nsmb.1507

Yang, H., G. Zhang, and J. Cui. 2015. BK channels: multiple sensors, one activation gate. *Front. Physiol.* 6:29. http://dx.doi.org/10.3389/fphys.2015.00029

Yang, J., G. Krishnamoorthy, A. Saxena, G. Zhang, J. Shi, H. Yang, K. Delaloye, D. Sept, and J. Cui. 2010. An epilepsy/dyskinesia-associated mutation enhances BK channel activation by potentiating Ca^{2+} sensing. *Neuron.* 66:871–883. http://dx.doi.org/10.1016/j.neuron.2010.05.009

Yang, J., H. Yang, X. Sun, K. Delaloye, X. Yang, A. Moller, J. Shi, and J. Cui. 2013. Interaction between residues in the Mg^{2+}-binding

site regulates BK channel activation. *J. Gen. Physiol.* 141:217–228. http://dx.doi.org/10.1085/jgp.201210794

Yuan, P., M.D. Leonetti, A.R. Pico, Y. Hsiung, and R. MacKinnon. 2010. Structure of the human BK channel Ca^{2+}-activation apparatus at 3.0 Å resolution. *Science.* 329:182–186. http://dx.doi.org/10.1126/science.1190414

Yuan, P., M.D. Leonetti, Y. Hsiung, and R. MacKinnon. 2011. Open structure of the Ca^{2+} gating ring in the high-conductance Ca^{2+}-activated K^+ channel. *Nature.* 481:94–97. http://dx.doi.org/10.1038/nature10670

Zhang, G., S.-Y. Huang, J. Yang, J. Shi, X. Yang, A. Moller, X. Zou, and J. Cui. 2010. Ion sensing in the RCK1 domain of BK channels. *Proc. Natl. Acad. Sci. USA.* 107:18700–18705. http://dx.doi.org/10.1073/pnas.1010124107

Zhang, G., H. Yang, H. Liang, J. Yang, J. Shi, K. McFarland, Y. Chen, and J. Cui. 2014. A charged residue in S4 regulates coupling among the activation gate, voltage, and Ca^{2+} sensors in BK channels. *J. Neurosci.* 34:12280–12288. http://dx.doi.org/10.1523/JNEUROSCI.1174-14.2014